BAREKENG: Journal of Mathematics and Its Applications
December 2025 Volume 19 Issue 4 Page 2419–2430
P-ISSN: 1978-7227 E-ISSN: 2615-3017
https://doi.org/10.30598/barekengvol19iss4pp2419-2430

MODELLING AND NUMERICAL ANALYSIS FOR CRACK PROPAGATION IN COMBINING CONCRETE WITH 25% FEATHER SHELL POWDER USING FINITE ELEMENT METHOD

Marah Doly Nasution[1], Muhammad Romi Syahputra[2*], Isnaini Halimah Rambe[3]

[1]*Mathematics Program, Universitas Muhammadiyah Sumatera Utara*
Jln. Muchtar Basri, Medan, 20238, Indonesia.

[2]*Mathematics Program, Faculty of Mathematics and Natural Sciences, Universitas Sumatera Utara*
Jln. Bioteknologi 1, Medan, 20155, Indonesia.

[3]*Mathematics Education Study Program, Universitas Islam Sumatera Utara*
Jln. Sisingamangaraja XII, Medan, 20217, Indonesia.

*Corresponding author's e-mail: * **m.romi@usu.ac.id***

Article History:

Received: 20th December 2024
Revised: 9th April 2025
Accepted: 10th June 2025
Available online: 1st September 2025

Keywords:

Concrete;
Crack Growth;
Crack Propagation,
Engineering Field;
Feather Shell Powder;
Finite Element Method;
Linear Triangle Element.
.

ABSTRACT

This study explores the application of the Extended Finite Element Method (XFEM) for modeling fracture behavior, utilizing COMSOL Multiphysics 5.6 to simulate a homogeneous concrete medium without embedded reinforcement. The computational model incorporates key parameters such as stress ratio (Young's modulus of 137.9 MPa), lateral strain from axial loading (Poisson's ratio of 0.17), concrete density of 2.4 g/cm³, and a crack growth rate governed by Paris' law. The simulation results show a maximum stress intensity factor (K_{max}) of 66.2 $Mpa \times m^{5\times10^{-1}}$ and a failure point occurring after approximately 22,568 load cycles. A mixture comprising 25% clamshell ash and lime was used as a sustainable cement substitute, achieving a maximum compressive strength of 20.53 MPa—meeting the structural concrete standard. These findings contribute to enhancing predictive fracture models and promoting sustainable material innovation in civil engineering.

How to cite this article:

M. D. Nasution, M. R. Syahputra and I. H. Rambe., "MODELLING AND NUMERICAL ANALYSIS FOR CRACK PROPAGATION IN COMBINING CONCRETE WITH 25% FEATHER SHELL POWDER USING FINITE ELEMENT METHOD," *BAREKENG: J. Math. & App.*, vol. 19, no. 4, pp. 2419-2430, December, 2025.

Journal homepage: *https://ojs3.unpatti.ac.id/index.php/barekeng/*
Journal e-mail: *barekeng.math@yahoo.com; barekeng.journal@mail.unpatti.ac.id*

Research Article · Open Access

1. INTRODUCTION

In modern structural engineering, concrete remains one of the most widely used construction materials due to its strength and versatility. However, conventional concrete production heavily relies on cement, which contributes significantly to global carbon emissions [1]. At the same time, increasing urban development has led to the generation of substantial industrial and organic waste. One such waste product is clamshell ash, which is typically discarded and underutilized. Recent studies have begun exploring the potential of incorporating waste materials into concrete to enhance sustainability and reduce environmental impact [2], [3][4].

Despite various studies investigating crack propagation in concrete using the Extended Finite Element Method (XFEM) [5][6][7], most of them focus on standard cement-based mixtures or reinforced concrete, with limited attention given to alternative sustainable mixtures such as those incorporating clamshell ash or elasto-plastic hydraulic fracture [8]. Moreover, while XFEM has been widely adopted for simulating fracture mechanics [9], there remains a research gap in combining this method with simulation tools like COMSOL Multiphysics to evaluate eco-friendly concrete mixtures.

The finite element method is a numerical technique that aims to overcome the limitations of mesh-related defects by extending the classical finite element approach to a mesh-independent framework [5][6]. While the Finite Element Method (FEM) and the Finite Volume Method (FVM) are both widely used for solving partial differential equations in engineering applications, they differ fundamentally in their approaches. FEM discretizes the problem domain into elements and uses interpolation functions to approximate the solution, making it well-suited for problems involving complex geometries and stress-strain analysis. In contrast, FVM is based on the conservation laws over control volumes and ensures local conservation of fluxes, which is particularly advantageous for fluid dynamics and heat transfer problems. As noted by [11], FVM emphasizes the balance of physical quantities across volumes, offering robust accuracy in modeling transport phenomena. The use of this technique in simulating cracks is anticipated to improve the representation of the environment surrounding the crack's tip and allow for the utilization of sophisticated global failure criteria that are designed specifically for engineering challenges, such as fracture behavior modeling [7]. The objective of this study is to investigate the utilization of the extended finite element method (XFEM) in modeling fracture behavior, with a specific emphasis on bare-bones concrete modeled using the COMSOL Multiphysics 5.6 software. The XFEM technique integrates various factors, such as stress ratios, lateral strains caused by axial loads, concrete density, and the rate of crack propagation, to simulate the crack growth mechanism [12], which extends the initial attachment as the crack size expands [13][14].

The accelerated expansion of the crack is linked to the stress intensity factor at the crack tip, which rises as the crack size increases, causing faster growth until it reaches a critical magnitude and breaks [15], [16]. The test reveals that the failure took place when the stress intensity surpassed the critical value, which is demonstrated by the comparison of the stress period and crack size. The growth rate of a crack is accelerated by the expansion of its size, which has a direct correlation, primarily influenced by the stress level factor at the tip of the crack [17][18][19].

This study aims to address this gap by analyzing the fracture behavior of concrete partially substituted with 25% clamshell ash using XFEM within COMSOL Multiphysics 5.6. The research evaluates crack propagation parameters such as stress ratio, lateral strain, and crack growth rate under axial loading. By integrating a sustainable material with advanced numerical simulation, this work not only contributes to fracture mechanics literature but also promotes environmental sustainability through waste utilization. The findings are expected to support future innovations in green construction materials and predictive modeling techniques.

The novelty and main contributions of this study can be summarized as follows:

1. This research investigates crack propagation behavior in concrete partially substituted with 25% clamshell ash—a type of marine biowaste—an area that has received very limited attention in fracture mechanics literature.
2. The study applies the Extended Finite Element Method (XFEM) using COMSOL Multiphysics 5.6, providing a mesh-independent simulation framework specifically tailored for eco-concrete, which is rarely implemented in prior works.

3. The integration of sustainability and computational fracture analysis presents a unique interdisciplinary contribution, addressing both environmental challenges and structural performance in construction materials.
4. The study contributes to the growing need for predictive modeling in sustainable infrastructure development by offering a replicable XFEM framework for future studies involving green construction materials.

The remainder of this paper is organized as follows: Section 2 presents the mathematical modeling and finite element formulation used in this study. Section 3 discusses the simulation results and their interpretation. Section 4 provides the conclusions drawn from the findings.

2. RESEARCH METHOD

2.1 Linear Triangle Elements

Linear triangular elements are planar elements with three nodes whose size varies linearly in the Cartesian coordinates of the x and y axes. In a stress analysis, the resulting linear displacement region is in the constant strain region, so this element is also called a CST element or Constant Strain Triangular element. **Figure 1** illustrates the basic configuration of a three-node linear triangular element, which is a fundamental component in the finite element method used in this study. This element type enables the approximation of displacement and stress distribution in a planar domain and is especially suitable for modeling irregular geometries such as those encountered in concrete fracture problems. In the finite element method for solving elliptic partial differential equations, the stiffness matrix denotes the linear system of equations that FEM needs to solve in order to approximate the solution to the differential equation. FEM is a numerical solution technique specifically made for solving engineering problems **[20]**.

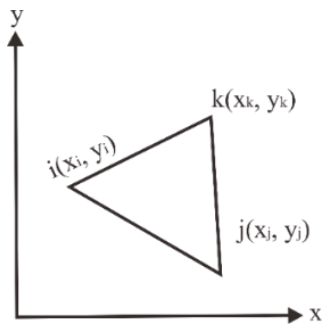

Figure 1. Three-Point Linear Triangle Element.

Figure 2 shows the application of linear triangular elements to represent a material domain under analysis. This visualization highlights how the geometry is discretized into small, manageable elements, forming the basis for applying XFEM techniques in simulating crack initiation and propagation. The arrangement also helps demonstrate how cracks can propagate through the mesh, independent of element boundaries.

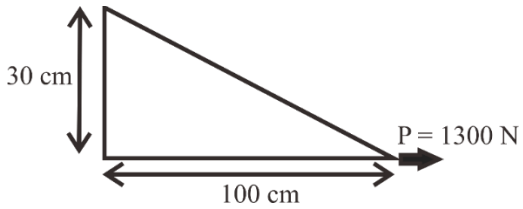

Figure 2. Triangular Linear Elements on a Material

Before examining all elements of a three-node triangle (CST), we will first discuss the definitions of plane stress and plane strain. The relationship between the strain and displacement of the plate is as **Equation (1)** to **Equation (2)**:

$$[\varepsilon] = \begin{bmatrix} \varepsilon_x \\ \varepsilon_y \\ \gamma_{xy} \end{bmatrix} = \begin{bmatrix} \frac{\partial_u}{\partial_x} & \frac{\partial_v}{\partial_y} & \frac{\partial_u}{\partial_y} + & \frac{\partial_v}{\partial_x} \end{bmatrix}^T \quad (1)$$

$$[\varepsilon] = [B][d] \quad (2)$$

ε_x : strain in the x direction

ε_y : strain in the y direction

γ_{xy} : shear strain in the xy plane

u : displacement in the x direction

v : displacement in the y direction

$\frac{\partial}{\partial_x}, \frac{\partial}{\partial_y}$: partial derivatives in the direction of x and y indicating changes in the displacement field

B : strain matrix

d : displacement matrix

σ_x : tension in the x direction

σ_y : tension in the y direction

σ_{xy} : shear tension in the xy plane

E : Young's modulus

v : Poisson's ratio - the ratio of lateral strain to axial strain

Equation (1) and **Equation (2)** represents the standard strain-displacement relation in plane stress conditions, commonly used in structural mechanics, where the relationship between stress and tension can be written as:

$$[\sigma] = [\mathrm{E}][\varepsilon] \quad (3)$$

Equation (3) is derived from Hooke's Law in two dimensions assuming isotropic and homogeneous material properties where the stress components are expressed as **Equation (4)**:

$$[\sigma] = \begin{bmatrix} \sigma_x \\ \sigma_y \\ \tau_{xy} \end{bmatrix} \quad (4)$$

In addition, the matrix [E] can calculate the plane stress area with **Equation (5)** and the plane strain area with **Equation (6)**.

$$[E] = \frac{E}{1-v^2} \begin{bmatrix} 1 & v & 0 \\ v & 1 & 0 \\ 0 & 0 & \frac{1-v}{2} \end{bmatrix} \quad (5)$$

$$[E] = \frac{E}{(1-v^2)(1-2v)} \begin{bmatrix} 1-v & v & 0 \\ v & 1-v & 0 \\ 0 & 0 & \frac{1-2v}{2} \end{bmatrix} \quad (6)$$

Equation (3) can also be written in the form of the following equation by substituting **Equation (2)**,

$$[\sigma] = [E][B][d] \quad (7)$$

2.2 General Equation of Linear Triangle Elements

The general equation for the transition matrix of a three-node linear triangle element is shown as **Equation (8)**:

$$[d] = \begin{bmatrix} d_i \\ d_j \\ d_m \end{bmatrix} = \begin{bmatrix} u_i \\ v_i \\ u_j \\ v_j \\ u_k \\ v_k \end{bmatrix} \tag{8}$$

here the transformation function can be defined as a linear transformation as follows:

$$u(x,y) = a_1 + a_2 x + a_3 y \tag{9}$$

$$u(x,y) = a_4 + a_5 x + a_6 y \tag{10}$$

According to the general transfer function $[\psi]$, **Equation (9)** and **Equation (10)** can be written as **Equation (11)**:

$$[\psi] = \begin{bmatrix} a_1 & a_2 x & a_3 y \\ a_4 & a_5 x & a_6 y \end{bmatrix} = \begin{bmatrix} 1 & x & y & 0 & 0 & 0 \\ 0 & 0 & 0 & 1 & x & y \end{bmatrix} \begin{bmatrix} a_1 \\ a_2 \\ a_3 \\ a_4 \\ a_5 \\ a_6 \end{bmatrix} \tag{11}$$

Then, to get the values of a_1 to a_6, first substitute the coordinates of the nodes into **Equation (12)**:

$$\begin{aligned} u_i &= a_1 + a_2 x_i + a_3 y_i \\ u_j &= a_1 + a_2 x_j + a_3 y_j \\ u_k &= a_1 + a_2 x_k + a_3 y_k \\ v_i &= a_4 + a_5 x_i + a_6 y_i \\ v_j &= a_4 + a_5 x_j + a_6 y_j \\ v_k &= a_4 + a_5 x_k + a_6 y_k \end{aligned} \tag{12}$$

Where $u_i = u(x_i, y_i)$ and $u_j = (x_j, y_j)$

$$\begin{bmatrix} u_i \\ u_j \\ u_k \end{bmatrix} = \begin{bmatrix} 1 & x_i & y_i \\ 1 & x_j & y_j \\ 1 & x_k & y_k \end{bmatrix} \begin{bmatrix} a_1 \\ a_2 \\ a_3 \end{bmatrix}$$

$$[a] = [x]^{-1}[u]$$

$$[x]^{-1} = \frac{1}{2A} \begin{bmatrix} \alpha_i & \alpha_j & \alpha_k \\ \beta_i & \beta_j & \beta_k \\ \gamma_i & \gamma_j & \gamma_k \end{bmatrix}$$

$$2A = \begin{bmatrix} 1 & x_i & y_i \\ 1 & x_j & y_j \\ 1 & x_k & y_k \end{bmatrix}$$

$$2A = x_i(y_i - y_k) + x_j(y_k - y_i) + x_k(y_i - y_j) \tag{12}$$

From **Equation (12)** we obtain A is the area of the triangle.

$$\begin{aligned} a_i &= x_j y_k - y_j x_k \\ a_j &= x_k y_i - y_k x_i \\ a_k &= x_i y_i - y_i \\ \beta_i &= y_j - y_k \\ \beta_j &= y_k - y_j \\ \beta_k &= y_i - yj \\ \gamma_i &= x_k - x_j \\ \gamma_j &= x_i - x_k \\ \gamma_k &= x_j - x_i \end{aligned} \tag{14}$$

In this study, α, β, and γ represent the interpolation coefficients derived from nodal coordinates of triangular elements, used to construct the shape functions in the finite element formulation. **Equation (14)** represents the general form of the interpolation function for a three-node linear triangular element, which is essential in the finite element method for constructing shape functions. This equation is derived by substituting the nodal coordinates into the linear transformation functions, resulting in the interpolation coefficients α, β, and γ. These coefficients are used to relate the displacement within the element to the global coordinate system. The formulation plays a crucial role in generating the stiffness matrix and analyzing the mechanical response of the material under applied loading.

2.3 The XFEM Algorithm

The computational procedure for modeling crack propagation using the Extended Finite Element Method (XFEM) in COMSOL Multiphysics is outlined through the following algorithm:

Algorithm: XFEM-based Crack Propagation Simulation

1. **Initialize the model** by defining the geometry of the concrete specimen, including the initial crack location and dimensions.
2. **Assign material properties** to the domain, such as Young's modulus (E), Poisson's ratio (ν), density, and fatigue parameters from Paris' law (C and m).
3. **Generate the mesh** using linear triangular elements/ Constant Strain Triangular (CST) element, ensuring adequate refinement around the crack tip region.
4. **Apply boundary conditions** and define the axial load cycles, specifying maximum and minimum tensile and bending stresses.
5. **Activate XFEM settings** in the solid mechanics module to allow discontinuity modeling independent of mesh topology.
6. **Implement Paris' Law** for fatigue crack growth to define the relationship between crack growth rate and Stress Intensity Factor (SIF).
7. **Run the simulation iteratively**, updating the crack length and position based on computed SIF values at each cycle.
8. **Evaluate the failure condition**: if the computed SIF reaches or exceeds the critical threshold K_{Ic}, terminate the simulation.
9. **Record the output results**, including stress intensity values, crack length progression, deformation contours, and number of cycles to failure.

This algorithm enables efficient tracking of crack evolution and material degradation under cyclic loading, providing insights into the fracture behavior of sustainable concrete materials.

3. RESULTS AND DISCUSSION

The numerical results presented in this section are obtained by solving the crack propagation model described in Section 2 using COMSOL Multiphysics 5.6. The simulation is grounded on the mathematical formulations derived from the linear triangular element method and the extended finite element framework,

including the strain-displacement relationship (**Equation (1)** to **Equation (2)**), stress-strain matrix (**Equation (3)** to **Equation (6)**), and interpolation functions for CST elements (**Equation (8)** to **Equation (14)**). These equations are embedded within the software's solver, which iteratively computes the stress intensity factor (SIF) and crack growth behavior in accordance with Paris' law.

Thus, although the software executes the numerical computations, the underlying process strictly follows the mathematical structure developed in the modeling stage, ensuring that the simulation results are a direct consequence of the equations previously formulated.

The stress ratio (Young's modulus) of 2.75×10^4 Mpa, lateral strain due to axial loading (Poisson ratio) of 0.17, and Concrete Density (Density) of 2.4 $\mathrm{g/cm^3}$ are specified before performing the calculation. In the laboratory test, the material under investigation had a crack growth rate (Paris' law coefficient) of 1.4×10^{-11} and was characterized by the dimensions of Length 100cm, Width 30cm, Thickness 25cm, and an initial crack of 1cm. The results indicate the upper limit of loading cycles endured before material failure occurs, as presented below:

$$N_{\text{fail}} = 22568 \text{ cycles to failure}$$

An increase in crack size leads to a rise in the stress intensity factor at the crack tip. Failure is initiated once this value surpasses the critical intensity level of the material, denoted by K_{Ic}. The pressure intervals, as shown in **Table 1**, represent the loading history, which is cyclically applied until structural failure occurs.

Table 1. ***Stress History***

Cycles	Tensile Max	Tensile Min	Bending Max	Bending Min
100	137.9 Mpa	0.000 Mpa	68.85 Mpa	0.000 Mpa
125	68.95 Mpa	34.47 Mpa	0.000 Mpa	0.000 Mpa

The stress history involves 125 cycles. The total number of stress histories that can be repeated before the material fails is yet to be determined by:

$$X_{\text{hist}} = \frac{N_{\text{fail}}}{N_{\text{hist}}} = \\ = \frac{22568}{125} = 180.54 \approx 181 \text{ history repetitions to failure}$$

This indicates that the material underwent 181 distinct load cycles or propagation steps before reaching the critical stress intensity threshold, leading to structural failure. Each repetition in the X_{hist} record corresponds to a computed stage in the crack growth history, which is essential for understanding the fatigue behavior of the material under repeated stress.

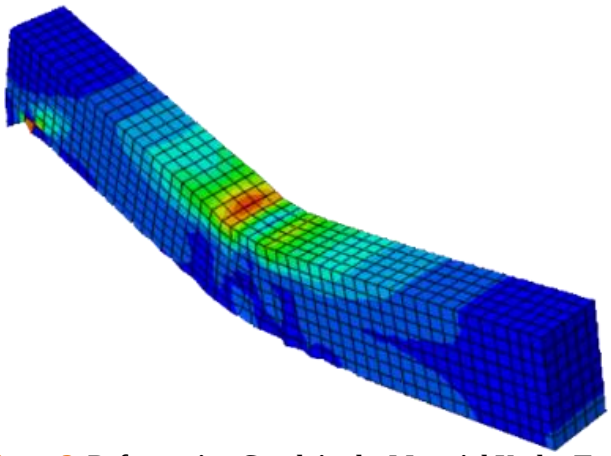

Figure 3. Deformation Crack in the Material Under Test.

Figure 3 illustrates the deformation field in the tested concrete specimen, simulated under axial loading using COMSOL Multiphysics 5.6 software. The deformation is concentrated around the crack tip, forming a localized high-strain region aligned with the direction of applied load. This result corresponds to a stress cycle near 18,000, where fatigue effects become more pronounced. The gradual increase in displacement reflects the accumulation of internal damage, and the deformation zone expands as the crack progresses.

These observations confirm the predicted behavior based on the increasing stress intensity factor, which drives crack propagation towards failure.

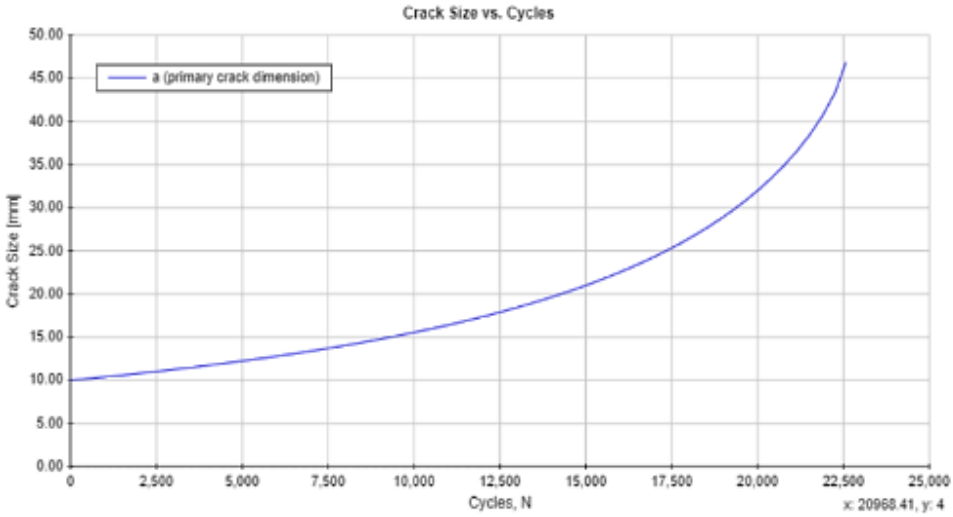

Figure 4. Crack Growth.

Cracks grow when the change in energy is greater than or equal to the resistance change. When the energy change is less than the resistance change, cracking will not occur. In tension, the maximum tension value is employed. Failure is determined by comparing the maximum stress intensity factor to K_{Ic}.

As can be seen from the crack growth process in **Figure 4**, the growth initially increases with the crack size. Finally, the growth $\left(\frac{da}{dN}\right)$ is faster. The crack grows more quickly because of the stress intensity factor (SIF) at the tip of the crack, which rises as the crack size increases. Until it reaches a critical size and ultimately fails, the crack will keep growing at an accelerated pace.

According to the test results, failure was caused by surpassing the critical stress intensity. **Figure 4** also illustrates a comparison of load cycling as crack size increases. The reason for the acceleration in growth is that the growth rate relies on the stress intensity factor at the crack tip, which, in turn, is dependent on the crack size.

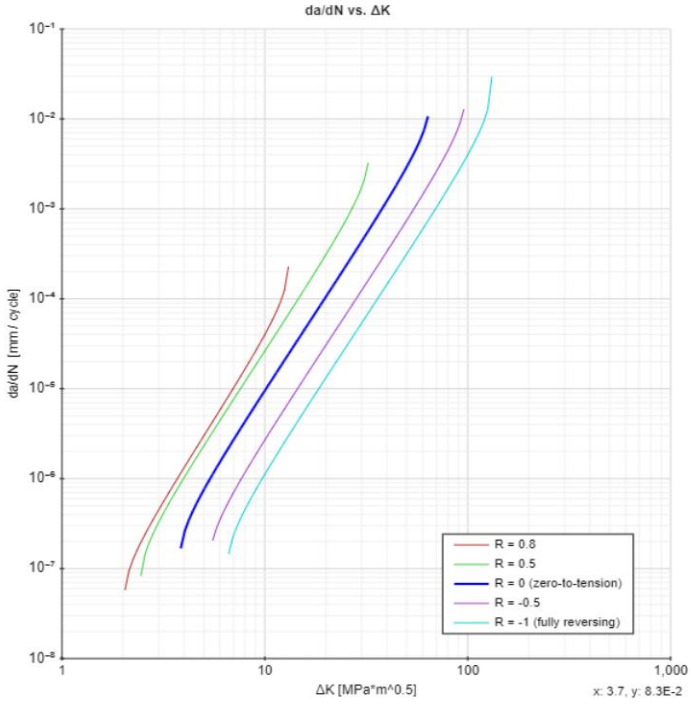

Figure 5. Crack Growth Rate as a Function of Stress Intensity Factor (ΔK) Based on Paris' Law

The graph in **Figure 5** shows the relationship between crack growth rate (da/dN) and the stress intensity factor (ΔK), illustrating the material's fatigue behavior under cyclic loading. As ΔK increases due to the enlarging crack, the rate of crack growth accelerates until it reaches a critical threshold. This plot quantifies the dynamic response of the material to stress cycles and complements the crack length progression illustrated in **Figure 4**.

The fracture toughness is linked to the thickness of the component. If the thickness rises, the fracture toughness declines to the stress level Fracture toughness K_{Ic}. **Figure 4** also illustrates the crack's orientation and the fracture's form in the examined material. When the material breaks, the analysis is concluded. The data sampling from the simulation results was done for 22,568 cycles with a maximum stress intensity factor (K_{max}) of 66.2 Mpa $\times$ m$^{5\times10^{-1}}$. **Figure 6** displays the sampling of the crack growth outcomes.

The stress intensity factor (SIF) distribution shown in **Figure 6** demonstrates a progressive increase in stress concentration near the crack tip, which governs the rate of crack propagation. As the crack lengthens under cyclic loading, the SIF exceeds the material's fracture toughness, leading to unstable crack growth. The simulation results indicate that the crack propagation follows the Paris law, where the growth rate is proportional to the applied stress intensity range. Additionally, the finite element analysis highlights the influence of mesh refinement on accurately capturing the stress singularity at the crack tip. The correlation between the numerical model and experimental data confirms the validity of the adopted fracture mechanics approach, emphasizing the role of stress distribution in predicting material failure.

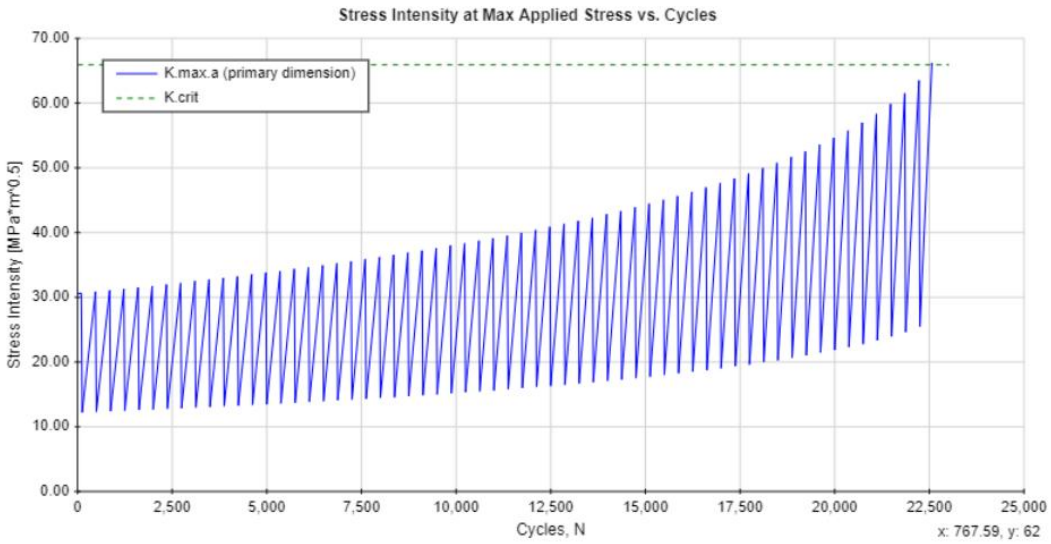

Figure 6. Stress Intensity

Figure 7 showcases how finite element analysis can be applied to simulate crack propagation in geometrically complex materials. The loading condition is quasi-cyclic, approximating static behavior, and the direction of crack extension is guided by the stress intensity factor values observed during the simulation process. The initial geometry comprises 1875 tetrahedral meshes, and the crack gap is positioned at the exact center of the material where crack growth is anticipated. In the simulation, the Paris fatigue law is employed, assuming that the crack propagation angle is the maximum hoop stress, as the fracture equation. A constant Δ_a is taken into consideration for each iteration to determine the change in crack length.

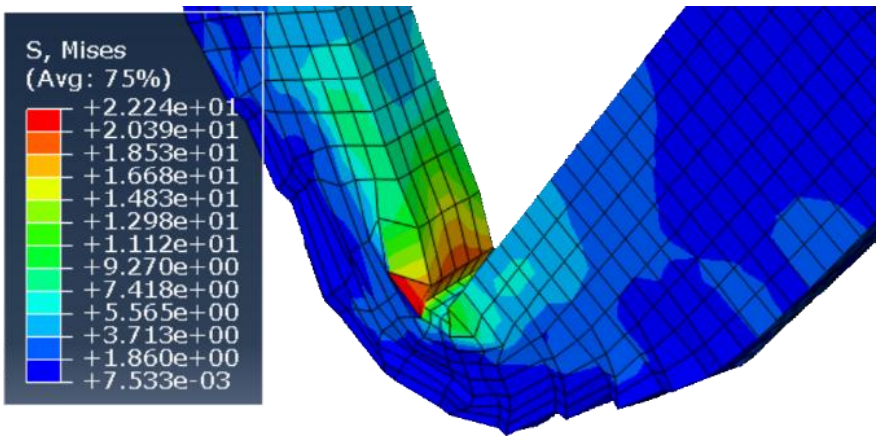

Figure 7. The Contour of Displacement Distribution along the Crack Path

Figure 7 also displays the displacement contour along the crack propagation path under quasi-static axial loading. The displacement field indicates that the deformation is highly localized at the crack tip, where the material experiences maximum displacement. This visualization confirms that the crack initiates and extends in the direction of the highest strain energy density, aligned with the applied load. The smooth gradient of the contour illustrates the gradual energy transfer through the material until the critical displacement threshold is reached. These results validate the use of XFEM in predicting displacement behavior in heterogeneous materials such as clamshell-ash-based concrete.

4. CONCLUSION

This study presents a numerical analysis of crack propagation in concrete incorporating 25% clamshell ash as a sustainable partial cement replacement, using the Extended Finite Element Method (XFEM) implemented in COMSOL Multiphysics 5.6. The following conclusions can be drawn:

1. The integration of clamshell ash as a cement substitute enhances the mechanical performance of concrete. The maximum compressive strength achieved was 20.53 MPa, which satisfies the structural standard for concrete applications.
2. Simulation results confirm that crack propagation behavior in the tested material is governed by Paris' law, where the crack growth rate increases non-linearly with the stress intensity factor. The model showed a maximum stress intensity factor of 66.2 and a failure point after approximately 22,568 loading cycles.
3. The finite element simulation effectively captured the deformation patterns and stress intensity distributions around the crack tip. As the crack size increased, the corresponding stress intensity factor also rose, resulting in accelerated crack growth and eventual failure once the critical threshold was exceeded.
4. A higher substitution ratio of clamshell ash and lime is associated with increased porosity, which may reduce both compressive and tensile strengths. This highlights the need for optimized mix design when utilizing waste-based materials in structural applications.
5. The XFEM-based approach provided a mesh-independent and robust framework for predicting crack growth in eco-concrete. The findings underscore the potential of combining sustainable materials with advanced numerical modeling to improve structural reliability while supporting green construction initiatives.

Future research may expand on this model by incorporating more complex loading scenarios, reinforced concrete behavior, or hybrid material compositions to further validate and generalize the proposed methodology.

AUTHOR CONTRIBUTIONS

Marah Doly Nasution: Conceptualization, Funding Acquisition. Muhammad Romi Syahputra: Methodology, Software, Writing-Review and Editing. Isnaini Halimah Rambe: Formal Analysis, Validation. All authors discussed the results and contributed to the final manuscript.

FUNDING STATEMENT

This research received no specific grant from any funding agency in the public, commercial, or not for profit sectors.

ACKNOWLEDGMENT

The authors would like to express their sincere gratitude to all co-authors for their valuable contributions to the preparation and completion of this article. Special thanks are also extended to the students who assisted in the data collection and processing, whose support was instrumental to the success of this research.

CONFLICT OF INTEREST

The authors declare that there is no conflict of interest among the authors related to this study.

REFERENCES

[1] J. Figueroa, M. Fuentealba, R. Ponce, and M. Zúñiga, "EFFECTS ON THE COMPRESSIVE STRENGTH AND THERMAL CONDUCTIVITY OF MASS CONCRETE BY THE REPLACEMENT OF FINE AGGREGATE BY MUSSEL SHELL PARTICULATE," *IOP Conf. Ser. Earth Environ. Sci.*, vol. 503, no. 1, p. 012070, May 2020, doi: https://doi.org/10.1088/1755-1315/503/1/012070.

[2] R. Karolina, A. S. Rezeki, Syahrizal, and M. A. P. Handana, "THE EFFECT OF CLAMSHELL ASH SUBSTITUTION TO THE MECHANICAL PROPERTIES OF CONCRETE," in *IOP Conference Series: Materials Science and Engineering*, Institute of Physics Publishing, Oct. 2019. doi: https://doi.org/10.1088/1757-899X/648/1/012045.

[3] W. Demin and H. Fukang, "INVESTIGATION FOR PLASTIC DAMAGE CONSTITUTIVE MODELS OF THE CONCRETE MATERIAL," *Procedia Eng.*, vol. 210, pp. 71–78, 2017, doi: https://doi.org/10.1016/j.proeng.2017.11.050.

[4] D. Wang, Q. Zhao, C. Yang, Y. Chi, W. Qi, and Z. Teng, "STUDY ON FROST RESISTANCE AND VEGETATION PERFORMANCE OF SEASHELL WASTE PERVIOUS CONCRETE IN COLD AREA," *Constr. Build. Mater.*, vol. 265, p. 120758, Dec. 2020, doi: https://doi.org/10.1016/j.conbuildmat.2020.120758.

[5] S. Liang, Y. Zhu, M. Huang, and Z. Li, "SIMULATION ON CRACK PROPAGATION VS. CRACK-TIP DISLOCATION EMISSION BY XFEM-BASED DDD SCHEME," *Int. J. Plast.*, vol. 114, no. October 2018, pp. 87–105, 2019, doi: https://doi.org/10.1016/j.ijplas.2018.10.010.

[6] B. Chen, "FINITE ELEMENT STRENGTH REDUCTION ANALYSIS ON SLOPE STABILITY BASED ON ANSYS," *Environ. Earth Sci. Res. J.*, vol. 4, no. 3, pp. 60–65, Sep. 2017, doi: https://doi.org/10.18280/eesrj.040302.

[7] F. Meray, T. Chaise, A. Gravouil, P. Depouhon, B. Descharrieres, and D. Nélias, "A NOVEL SAM/X-FEM COUPLING APPROACH FOR THE SIMULATION OF 3D FATIGUE CRACK GROWTH UNDER ROLLING CONTACT LOADING," *Finite Elem. Anal. Des.*, vol. 206, no. April, p. 103752, 2022, doi: https://doi.org/10.1016/j.finel.2022.103752.

[8] W. Liu, Q. Zeng, J. Yao, Z. Liu, T. Li, and X. Yan, "NUMERICAL STUDY OF ELASTO-PLASTIC HYDRAULIC FRACTURE PROPAGATION IN DEEP RESERVOIRS USING A HYBRID EDFM–XFEM METHOD," *Energies*, vol. 14, no. 9, p. 2610, May 2021, doi: https://doi.org/10.3390/en14092610.

[9] Y. Zhou *et al.*, "A NUMERICAL METHOD TO CONSIDER THE INTERACTION BETWEEN MULTIPLE FRACTURES IN FROZEN ROCKS BASED ON XFEM," *Comput. Geotech.*, vol. 169, p. 106240, May 2024, doi: https://doi.org/10.1016/j.compgeo.2024.106240.

[10] A. Bergara, J. I. Dorado, A. Martin-Meizoso, and J. M. Martínez-Esnaola, "FATIGUE CRACK PROPAGATION IN COMPLEX STRESS FIELDS: EXPERIMENTS AND NUMERICAL SIMULATIONS USING THE EXTENDED FINITE ELEMENT METHOD (XFEM)," *Int. J. Fatigue*, vol. 103, pp. 112–121, 2017, doi: https://doi.org/10.1016/j.ijfatigue.2017.05.026.

[11] A. Fatahillah, A. D. Pratiwi, S. Setiawani, A. I. Kristiana, and R. Adawiyah, "NUMERICAL ANALYSIS IN ARTERIAL STENOSIS AFFECTED BY ISCHEMIC HEART DISEASE USING FINITE VOLUME METHOD," *BAREKENG J. Ilmu Mat. dan Terap.*, vol. 18, no. 1, pp. 0179–0192, Mar. 2024, doi: https://doi.org/10.30598/barekengvol18iss1pp0179-0192.

[12] I. S. Parvathi, M. Mahesh, and D. V. V. R. Kamal, "XFEM METHOD FOR CRACK PROPAGATION IN CONCRETE

GRAVITY DAMS," *J. Inst. Eng. Ser. A*, vol. 103, no. 2, pp. 677–687, Jun. 2022, doi: https://doi.org/10.1007/s40030-022-00636-2.

[13] M. R. Purba, T. Tulus, M. R. Syahputra, and S. Sawaluddin, "IMPLEMENTATION OF EXTENDED FINITE ELEMENT METHOD IN CRACK PROPAGATION OF CONCRETE," *J. Fundam. Math. Appl.*, vol. 5, no. 1, pp. 1–8, Jul. 2022, doi: https://doi.org/10.14710/jfma.v5i1.14454.

[14] K. Tazoe, H. Tanaka, M. Oka, and G. Yagawa, "AN APPROACH FOR FATIGUE CRACK PROPAGATION ANALYSIS BY SMOOTHED PARTICLE HYDRODYNAMICS METHOD," *Strength, Fract. Complex.*, vol. 12, no. 2–4, pp. 127–133, Mar. 2020, doi: https://doi.org/10.3233/SFC-190242.

[15] A. M. Singh and M. M. Sharma, "ANALYSIS ON FATIGUE CRACK INITIATION AND FATIGUE CRACK PROPAGATION IN A GEAR," *Smart Moves J. Ijoscience*, vol. 4, no. 7, p. 13, 2018, doi: https://doi.org/10.24113/ijoscience.v4i7.155.

[16] A. Jafari, P. Broumand, M. Vahab, and N. Khalili, "AN EXTENDED FINITE ELEMENT METHOD IMPLEMENTATION IN COMSOL MULTIPHYSICS: SOLID MECHANICS," *Finite Elem. Anal. Des.*, vol. 202, 2022, doi: https://doi.org/10.1016/j.finel.2021.103707.

[17] S. Sugito, S. W. Alisjahbana, and H. Riyanto, "MODELING OF MECHANICAL PERFORMANCE FROM CONCRETE MADE BY COMBINING IRON SAND AND GLASS POWDER FILLER UNDER HOT WATER CURING CONDITION," *Math. Model. Eng. Probl.*, vol. 9, no. 2, pp. 418–424, Apr. 2022, doi: https://doi.org/10.18280/mmep.090216.

[18] O. N. Stepanova, L., & Belova, "ESTIMATION OF CRACK PROPAGATION DIRECTION ANGLES UNDER MIXED MODE LOADING IN LINEAR ELASTIC ISOTROPIC MATERIALS BY GENERALIZED FRACTURE MECHANICS CRITERIA AND BY MOLECULAR DYNAMICS METHOD ESTIMATION OF CRACK PROPAGATION DIRECTION ANGLES UNDER MIXED MODE l," *J. Phys. Conf. Ser.*, vol. 1096, p. 012060, 2018, doi: https://doi.org/10.1088/1742-6596/1096/1/012060.

[19] Y. Zhang, Z. Gao, Y. Li, and X. Zhuang, "ON THE CRACK OPENING AND ENERGY DISSIPATION IN A CONTINUUM BASED DISCONNECTED CRACK MODEL," *Finite Elem. Anal. Des.*, vol. 170, no. June 2019, p. 103333, 2020, doi: https://doi.org/10.1016/j.finel.2019.103333.

[20] X. Q. Nguyen, T. T. Banh, and D. Lee, "A CONSTANT STRAIN TRIANGLE ELEMENT ORIENTED MULTI-MATERIAL TOPOLOGY OPTIMIZATION WITH A MOVED AND REGULARIZED HEAVISIDE FUNCTION," *Struct. Eng. Mech.*, vol. 79, no. 01, pp. 97–107, 2021, doi: https://doi.org/10.12989/sem.2021.79.1.097.